J|A|C|S
ARTICLES
Published on Web 10/14/2004

Deciphering the Origins of Observed Heat Capacity Changes for Aminoglycoside Binding to Prokaryotic and Eukaryotic Ribosomal RNA A-Sites: A Calorimetric, Computational, and Osmotic Stress Study

Christopher M. Barbieri, Annankoil R. Srinivasan, and Daniel S. Pilch*

Contribution from the Department of Pharmacology, University of Medicine and Dentistry of New Jersey, Robert Wood Johnson Medical School, 675 Hoes Lane, Piscataway, New Jersey 08854-5635

Received July 15, 2004; E-mail: pilchds@umdnj.edu

Abstract: Isothermal titration calorimetry (ITC), computational, and osmotic stress techniques have been used to characterize the changes in heat capacity, solvent-accessible surface, and hydration that accompany the binding of the aminoglycoside paromomycin to both prokaryotic and eukaryotic rRNA A-site model oligonucleotides. Regarded as a whole, the results of these studies suggest that the intrinsic heat capacity change (ΔC_p) for the binding of paromomycin to each rRNA A-site is near zero, with the negative ΔC_p observed for the binding of the drug to the prokaryotic rRNA A-site being dictated by the coupled destacking of the adenine residues at positions 1492 and 1493. In this connection, ΔC_p provides a useful calorimetric signature for assessing the relative impacts of novel and existing A-site targeting ligands on rRNA conformation, which, in turn, should provide a useful analytical tool for facilitating the drug design process, since aminoglycoside-induced destacking of A1492 and A1493 is thought to be a determining factor in the mistranslational and antimicrobial activities of the drugs.

Introduction

An understanding of the molecular forces that govern the affinities and specificities of drugs for their macromolecular targets requires the integration of thermodynamic and structural information. The increasing availability of high-resolution structural information for many drug−macromolecule complexes has yielded important insights into the relationship between structure and energetics. One of the more challenging aspects of this relationship has been the molecular interpretation of observed heat capacity changes (ΔC_p) for drug−macromolecule interactions. This task is complicated by the numerous potential factors that can contribute to observed heat capacity changes.[1−13] These factors include (i) the hydrophobic effect that stems from the release of constrained water molecules accompanying the burial of nonpolar surfaces,[2−6,10] (ii) the alteration of "soft" internal vibrational modes at polar interfaces that accompanies the binding reaction, [1,7,13] (iii) electrostatic interactions,[11] and (iv) the coupling or linkage of temperature-dependent equilibria (e.g., conformational changes and protonation reactions) to the binding reaction.[1,7−9,12]

For numerous protein folding,[2−4,6] protein−protein,[5] and drug−DNA interactions,[10,14,15] correlations have been reported between experimentally observed ΔC_p values and those calculated based on the burial of solvent-accessible surfaces, with the burial of nonpolar surfaces resulting in a negative contribution to ΔC_p and the burial of polar surfaces resulting in a positive contribution to ΔC_p. However, in several recent studies of protein−DNA interactions, the experimental and calculated ΔC_p values do not agree.[7,13,16−20] In each of these cases, the observed ΔC_p was greater in magnitude than the corresponding calculated value, with this discrepancy being attributed to contributions to the observed ΔC_p from a binding-induced tightening of soft internal vibrational modes[13,17,18] at the protein−DNA interface

(1) Sturtevant, J. M. *Proc. Natl. Acad. Sci. U.S.A.* **1977**, *74*, 2236−2240.
(2) Spolar, R. S.; Livingstone, J. R.; Record, M. T., Jr. *Biochemistry* **1992**, *31*, 3947−3955.
(3) Spolar, R. S.; Record, M. T., Jr. *Science* **1994**, *263*, 777−784.
(4) Murphy, K. P.; Freire, E. *Adv. Protein Chem.* **1992**, *43*, 313−361.
(5) Gómez, J.; Hilser, V. J.; Xie, D.; Freire, E. *Proteins: Struct., Funct., Genet.* **1995**, *22*, 404−412.
(6) Habermann, S. M.; Murphy, K. P. *Protein Sci.* **1996**, *5*, 1229−1239.
(7) Kozlov, A. G.; Lohman, T. M. *Biochemistry* **1999**, *38*, 7388−7397.
(8) Holbrook, J. A.; Capp, M. W.; Saecker, R. M.; Record, M. T., Jr. *Biochemistry* **1999**, *38*, 8409−8422.
(9) Kozlov, A. G.; Lohman, T. M. *Proteins: Struct., Funct., Genet.* **2000**, *41*(S4), 8−22.
(10) Ren, J.; Jenkins, T. C.; Chaires, J. B. *Biochemistry* **2000**, *39*, 8439−8447.
(11) Sharp, K. A. In *Thermodynamics in Biology*; Di Cera, E., Ed.; Oxford University Press: New York, 2000; pp 113−130.
(12) Kaul, M.; Pilch, D. S. *Biochemistry* **2002**, *41*, 7695−7706.
(13) Bergqvist, S.; Williams, M. A.; O'Brien, R.; Ladbury, J. E. *J. Mol. Biol.* **2004**, *336*, 829−842.
(14) Haq, I.; Ladbury, J. E.; Chowdhry, B. Z.; Jenkins, T. C.; Chaires, J. B. *J. Mol. Biol.* **1997**, *271*, 244−257.
(15) Mazur, S.; Tanious, F. A.; Ding, D.; Kumar, A.; Boykin, D. W.; Simpson, I. J.; Neidle, S.; Wilson, W. D. *J. Mol. Biol.* **2000**, *300*, 321−337.
(16) Jin, L.; Yang, J.; Carey, J. *Biochemistry* **1993**, *32*, 7302−7309.
(17) Ladbury, J. E.; Wright, J. G.; Sturtevant, J. M.; Sigler, P. B. *J. Mol. Biol.* **1994**, *238*, 669−681.
(18) Berger, C.; Jelesarov, I.; Bosshard, H. R. *Biochemistry* **1996**, *35*, 14984−14991.
(19) O'Brien, R.; DeDecker, B.; Fleming, K. G.; Sigler, P. B.; Ladbury, J. E. *J. Mol. Biol.* **1998**, *279*, 117−125.
(20) Oda, M.; Furukawa, K.; Ogata, K.; Sarai, A.; Nakamura, H. *J. Mol. Biol.* **1998**, *276*, 571−590.

10.1021/ja0457516 CCC: $27.50

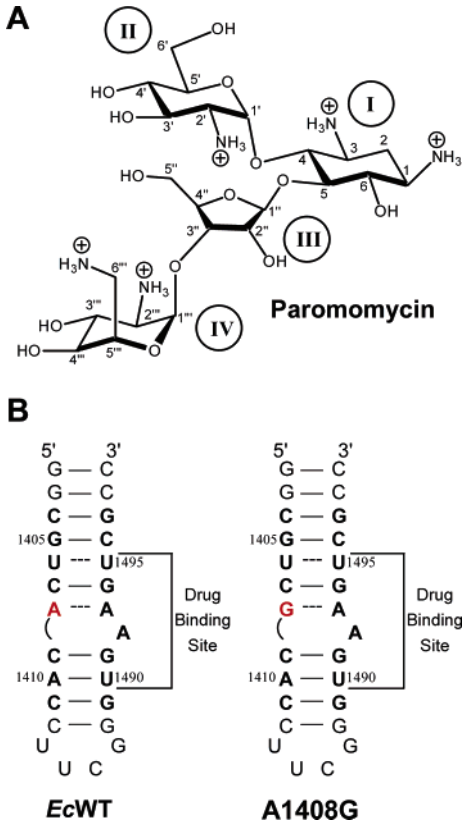

Figure 1. (A) Structure of paromomycin in its fully protonated pentacationic state, with the atomic and ring-numbering systems denoted in Arabic and Roman numerals, respectively. Ring I of this structure is 2-deoxystreptamine (2-DOS). (B) Secondary structures of the *E. coli* 16 S rRNA A-site model oligonucleotide (*Ec*WT) and its A1408G mutant (A1408G). Bases present in *E. coli* 16 S rRNA are depicted in bold face and are numbered as they are in 16 S rRNA. The base at position 1408, the identity of which distinguishes the two duplexes from each other, is depicted in red. The drug-binding site in each RNA (as revealed by NMR and footprinting studies[24,29,57,58]) is indicated.

or from binding-linked conformational changes in the protein[16,19,20] or DNA.[7]

A number of recent studies have demonstrated the impact that a coupled temperature-dependent process has on the observed ΔC_p for a binding reaction. In this connection, the observed ΔC_p for DNA duplex formation has been interpreted in terms of a coupling between the formation of "stacked" single-stranded DNA helices and the association of those helices to form a duplex.[8,21] Kozlov and Lohman[7] have demonstrated that the binding of *Escherichia coli* SSB protein to single-stranded oligo(dA) is coupled to the destacking of adenine bases, with this coupled destacking equilibrium dominating the observed negative ΔC_p for the binding reaction. The observed negative ΔC_p for the binding of SSB to single-stranded DNA has also been shown to reflect significant contributions from coupled protein protonation equilibria.[9]

We have previously shown that, at pH values >5.5, the binding of the aminoglycoside antibiotic paromomycin (Figure 1A) to an *E. coli* 16 S rRNA A-site model oligonucleotide (*Ec*WT) is coupled to drug protonation.[12,22] In addition, our studies have indicated that the binding-linked protonation of the drug makes significant contributions to the negative ΔC_p observed for the binding reaction.[12] However, even in the absence of drug protonation effects (i.e., at pH 5.5), the binding of paromomycin to *Ec*WT, whose secondary structure is depicted in Figure 1B, is still associated with a negative ΔC_p.[23] One of the hallmarks associated with the binding of paromomycin to the prokaryotic 16 S rRNA A-site is the coupled destacking of the adenine bases at positions 1492 and 1493 (Figure 1B).[24−28] The studies described here are designed to test the hypothesis that the observed negative ΔC_p that is associated with the paromomycin−*Ec*WT interaction in the absence of coupled drug protonation is a manifestation of the contributions from the destacking of A1492 and A1493 that is coupled to the binding reaction. To this end, we used isothermal titration calorimetry (ITC) over a range of temperatures (5−25 °C) to determine ΔC_p values for the binding of paromomycin to *Ec*WT and a mutant (A1408G) in which the adenine at position 1408 is replaced by guanine. We selected the A1408G mutant as a complementary drug target to *Ec*WT since recent studies have indicated that paromomycin binding to this mutant form of *Ec*WT is *not* associated with the destacking of A1492 and A1493 that is coupled to the paromomycin−*Ec*WT interaction.[28,29] Note that while prokaryotic rRNA A-sites contain an adenine at position 1408, eukaryotic A-sites contain a guanine at the equivalent position. Thus, *Ec*WT and A1408G represent model oligonucleotides for prokaryotic (16 S) and eukaryotic (18 S) rRNA A-sites, respectively. We compare calorimetrically derived ΔC_p values for the binding of paromomycin to *Ec*WT and A1408G with corresponding values calculated using recently proposed formalisms that are based on binding-induced changes in solvent-accessible surfaces. We also use a fluorescence-based osmotic stress approach to determine the hydration changes that accompany the paromomycin−*Ec*WT interaction. In the aggregate, our results suggest that the intrinsic ΔC_p for the paromomycin−*Ec*WT interaction is near zero, with the observed negative ΔC_p being dictated by the coupled destacking of A1492 and A1493.

Materials and Methods

RNA and Drug Molecules. The 27mer RNA oligonucleotides used in this study were obtained in their PAGE-purified sodium salt forms from Dharmacon Research, Inc. (Lafayette, CO). The concentrations of all RNA solutions were determined spectrophotometrically using the following extinction coefficients at 260 nm and 85 °C ($\epsilon_{260-85\ °C}$) [in units of (mol strand/L)$^{-1}$·cm^{-1}]:[28] $\epsilon_{260-85\ °C} = 253\,390 \pm 3170$ for *Ec*WT, $248\,370 \pm 940$ for *Ec*WT(2AP), and $256\,760 \pm 4490$ for A1408G. Paromomycin·H_2SO_4 was obtained from Fluka and was used without further purification.

Isothermal Titration Calorimetry (ITC). Isothermal calorimetric measurements were performed on a MicroCal VP−ITC (MicroCal, Inc.; Northampton, MA). Aliquots of paromomycin (10 μL) were injected from a 250 μL rotating syringe (300 rpm) into an isothermal sample chamber containing 1.42 mL of *Ec*WT or A1408G RNA solutions.

(21) Vesnaver, G.; Breslauer, K. J. *Proc. Natl. Acad. Sci. U.S.A.* **1991**, *88*, 3569−3573.
(22) Kaul, M.; Barbieri, C. M.; Kerrigan, J. E.; Pilch, D. S. *J. Mol. Biol.* **2003**, *326*, 1373−1387.
(23) Pilch, D. S.; Kaul, M.; Barbieri, C. M.; Kerrigan, J. E. *Biopolymers* **2003**, *70*, 58−79.
(24) Fourmy, D.; Recht, M. I.; Blanchard, S. C.; Puglisi, J. D. *Science* **1996**, *274*, 1367−1371.
(25) Fourmy, D.; Yoshizawa, S.; Puglisi, J. D. *J. Mol. Biol.* **1998**, *277*, 333−345.
(26) Carter, A. P.; Clemons, W. M.; Brodersen, D. E.; Morgan-Warren, R. J.; Wimberly, B. T.; Ramakrishnan, V. *Nature* **2000**, *407*, 340−348.
(27) Vicens, Q.; Westhof, E. *Structure* **2001**, *9*, 647−658.
(28) Kaul, M.; Barbieri, C. M.; Pilch, D. S. *J. Am. Chem. Soc.* **2004**, *126*, 3447−3453.
(29) Lynch, S. R.; Puglisi, J. D. *J. Mol. Biol.* **2001**, *306*, 1037−1058.

For each experiment, the paromomycin concentration was 500 μM and the RNA concentration was 20 μM in strand. Each experiment was accompanied by the corresponding control experiment in which 10 μL aliquots of the drug were injected into a solution of buffer alone. The duration of each injection was 10 s, and the initial delay prior to the first injection was 60 s. The delay between injections was 300 s. Each injection generated a heat burst curve (μcal/s vs s). The area under each curve was determined by integration [using the Origin version 7.0 software (MicroCal, Inc.; Northampton, MA)] to obtain a measure of the heat associated with that injection. The heat associated with each drug/buffer injection was subtracted from the corresponding heat associated with each drug/RNA injection to yield the heat of drug binding for that injection. Buffer conditions were 10 mM sodium cacodylate (pH 5.5) and 0.1 mM EDTA. Sufficient NaCl was added to the buffer solutions to bring the total Na^+ concentration to either 230 mM (for the titrations of paromomycin into *Ec*WT) or 150 mM (for the titrations of paromomycin into A1408G). The experiments with *Ec*WT were conducted at 5, 10, and 25 °C, while the experiments with A1408G were conducted at 5, 15, and 25 °C.

Calculation of Solvent-Accessible Surface Areas. All solvent-accessible surface areas were calculated using the GRASP version 1.3 software package[30] with a probe radius of 1.4 Å. The following NMR-derived solution structures obtained from the Protein Data Bank (PDB)[31] were used in these calculations: *Ec*WT alone[25] (PDB code 1a3m), *Ec*WT in complex with paromomycin[24] (PDB code 1pbr), A1408G alone[29] (PDB code 1fyo), and A1408G in complex with paromomycin[29] (PDB code 1fyp). The structure that best represented the average solution conformation was used in each calculation. Neither a solution structure nor a crystallographic structure of RNA-free paromomycin has been reported to date. Thus, for the purposes of calculating the solvent-accessible surface area of RNA-free paromomycin, we used the structure of paromomycin in its complex with either *Ec*WT or A1408G. Significantly, the solvent-accessible surface areas of the two RNA-free drug structures, so derived, were similar. Surfaces of carbon atoms, carbon-bound hydrogen atoms, and phosphorus atoms were defined as nonpolar. The surfaces of the remaining atoms (nitrogens, oxygens, and non-carbon-bound hydrogens) were defined as polar, except for the instances where the surfaces of hydroxyl functionalities were treated as a separate set.

Osmotic Stress Fluorescence Titrations. Steady-state fluorescence experiments were conducted on an AVIV Model ATF105 spectrofluorometer (Aviv Biomedical; Lakewood, NJ) equipped with a thermoelectrically controlled cell holder. A quartz cell with a 1 cm path length in both the excitation and emission directions was used in all of the experiments, which were conducted at 5 °C. The excitation and emission wavelengths were set at 310 and 370 nm, respectively. The excitation and emission slit widths were both set at 5 nm. In a typical experiment, 2−10 μL aliquots of 200 μM paromomycin were added to a solution of RNA that was 1 μM in strand. The added drug and RNA were allowed to equilibrate for 5 min, whereupon the fluorescence emission intensity was recorded over a 30 s interval and the average intensity determined. The ethylene glycol (>99.8% spectrophotometric grade) and glycerol (>99.5% spectrophotometric grade) used in the fluorescence experiments were obtained from Sigma-Aldrich. Experimental RNA and paromomycin solutions used in the fluorescence experiments were prepared via the following two-step procedure. (i) Appropriate aliquots of buffer and drug or buffer and RNA were combined and evaporated to dryness in a vacuum centrifuge. (ii) The dried pellets then were resuspended in the appropriate volume of osmolyte solution at the desired osmolality (Osm). The buffer conditions used in these experiments were 10 mM sodium cacodylate (pH 5.5), 0.1 mM EDTA, and sufficient NaCl to achieve a Na^+ concentration of 230 mM. When present, ethylene glycol was used at concentrations ranging from 0 to 6.2 Osm, and glycerol was used at concentrations ranging from 0 to 6.5 Osm. The osmolalities of all experimental solutions were measured using a freezing point depression osmometer (Osmette A model 5002; Precision Systems, Inc.).

UV Melting Studies. Temperature-dependent absorption experiments were conducted on an AVIV Model 14DS spectrophotometer (Aviv Biomedical; Lakewood, NJ) equipped with a thermoelectrically controlled cell holder. Quartz cells with a 1 cm path length were used for all of the absorbance studies. Temperature-dependent absorption profiles were acquired at 274 nm with a 6 s averaging time. The temperature was raised in 0.5 °C increments, and the samples were allowed to equilibrate for 1.5 min at each temperature setting. In these UV melting studies, the RNA solutions were 2 μM in strand. Buffer conditions and the method of experimental solution preparation were identical to those described above for the fluorescence titration experiments.

Circular Dichroism (CD) Measurements. CD measurements were acquired at 5 °C on an AVIV Model 202 spectropolarimeter equipped with a thermoelectrically controlled cell holder. A quartz cell with a 1 cm path length was used for all of the CD studies. CD spectra were acquired from 320 to 215 nm in 1 nm increments, with an averaging time of 3 s. In these studies, RNA concentrations were 3 μM in strand, with the buffer conditions and method of experimental solution preparation being identical to those described above for the fluorescence titration experiments.

Results and Discussion

Temperature-Dependent ITC Studies of Paromomycin Binding to *Ec*WT and A1408G. We used ITC to characterize the binding of paromomycin to *Ec*WT and A1408G at temperatures ranging from 5 to 25 °C. At pH values >5.5, paromomycin binding to *Ec*WT is thermodynamically linked to drug protonation.[12,22] We conducted our temperature-dependent ITC studies at pH 5.5, thereby eliminating contributions to the observed binding energetics from binding-linked drug protonation reactions. In addition to pH, ionic strength was also an important consideration for our ITC studies. We have previously shown that, at pH 5.5, the affinity of paromomycin for A1408G is more than an order of magnitude weaker than its affinity for *Ec*WT.[28] As a consequence of this differential affinity, we conducted our ITC studies with the A1408G duplex at an ionic strength ($[Na^+]$ = 150 mM) lower than that used in our corresponding studies with the *Ec*WT duplex ($[Na^+]$ = 230 mM). In this way, the unitless product of the binding constant (K) times the total starting duplex concentration times the binding stoichiometry (N) always fell within a range well suited for rigorous determination of the binding constant and the binding enthalpy (ΔH), regardless of the temperature employed. The ITC profiles resulting from our temperature-dependent ITC studies are shown in Figure 2. Each of the heat burst curves in panels A−C and E−G of Figure 2 corresponds to a single drug injection. The areas under these heat burst curves were determined by integration to yield the associated injection heats. These injection heats were corrected by subtraction of the corresponding dilution heats derived from the injection of identical amounts of drug into buffer alone. Panels D and H of Figure 2 show the resulting corrected injection heats plotted as a function of the [drug]/[duplex] ratio. Note that the ITC profiles for the binding of paromomycin to both host duplexes are biphasic, consistent with the presence of two binding equilibria. In each case, the first phase is significantly steeper than the second, an observation indicating that the binding constant for the first equilibrium is greater than that for the second. We have

(30) Nicholls, A.; Sharp, K. A.; Honig, B. *Proteins: Struct., Funct., Genet.* **1991**, *11*, 281−296.
(31) Berman, H. M.; Westbrook, J.; Feng, Z.; Gilliland, G.; Bhat, T. N.; Weissig, H.; Shindyalov, I. N.; Bourne, P. E. *Nucleic Acids Res.* **2000**, *28*, 235−242.

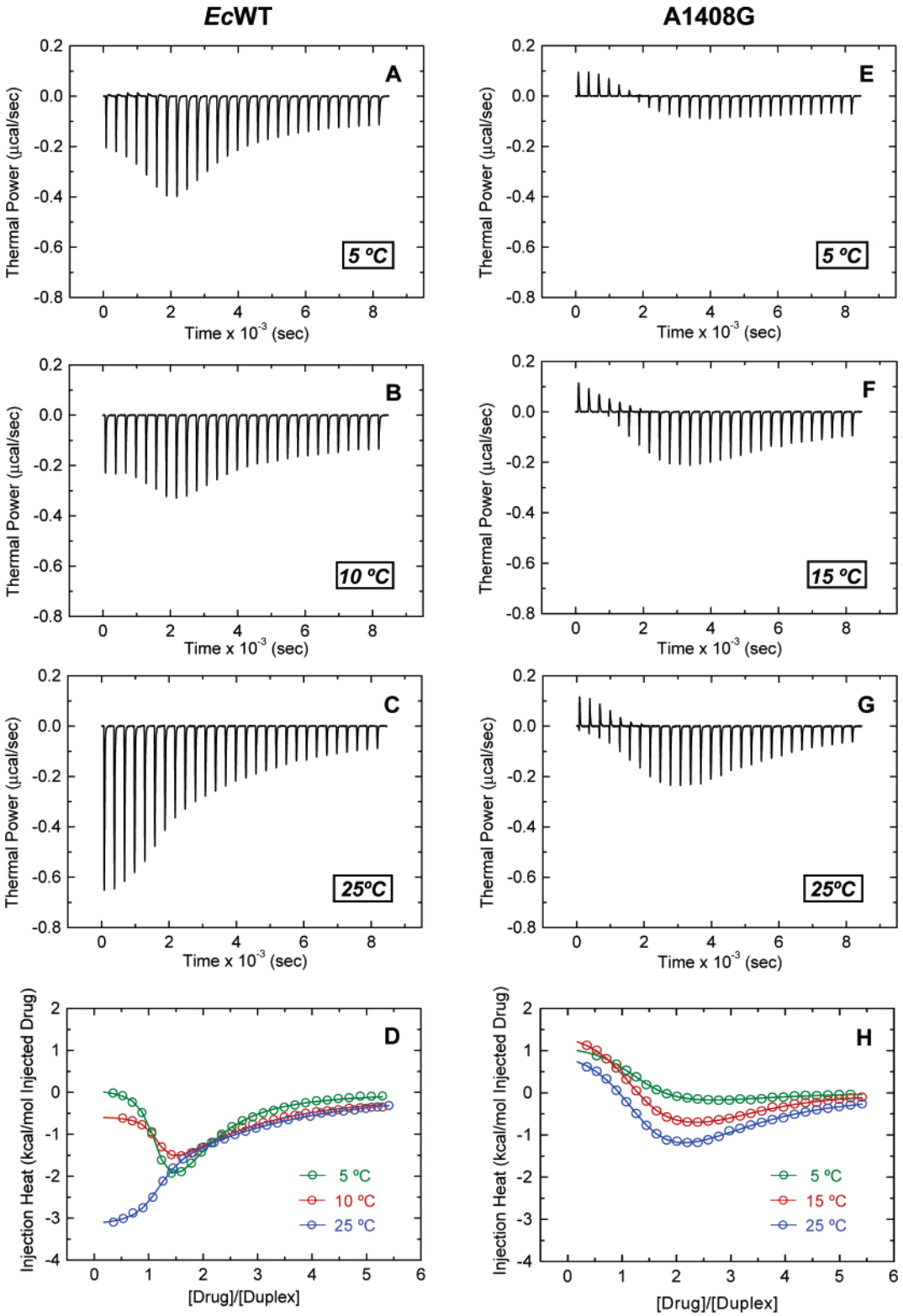

Figure 2. ITC profiles for the titration of paromomycin into a solution containing *Ec*WT (A−C) or A1408G (E−G) at pH 5.5 and temperatures ranging from 5 to 25 °C. Each of the heat burst curves in panels A−C and E−G is the result of a 10 μL injection of 500 μM paromomycin, with the RNA concentration being 20 μM in duplex. The corrected injection heats shown in panel D were derived by integration of the corresponding heat burst curves in panels A−C and followed by subtraction of the corresponding dilution heats derived from control titrations of drug into buffer alone. The corrected injection heats shown in panel H were derived in a similar fashion from the heat burst curves in panels E−G. The data points in panels D and H reflect the corrected experimental injection heats, while the solid lines reflect the calculated fits of the data using a model for two sets of binding sites. The temperature at which each titration was conducted is indicated. The buffer conditions for all titrations were 10 mM sodium cacodylate (pH 5.5) and 0.1 mM EDTA. Experimental solutions also contained sufficient NaCl to bring the total Na^+ concentration to either 230 mM (for *Ec*WT solutions) or 150 mM (for A1408G solutions).

previously assigned the first binding equilibrium to the specific A-site interaction observed in structural studies[24,26,27,29] and the second binding equilibrium to weaker nonspecific interactions.[12,22,28]

Table 1. Temperature Dependence of the ITC-Derived Interaction Parameters for the Binding of Paromomycin with the *Ec*WT and A1408G Duplexes at pH 5.5[a]

RNA	T (°C)	[Na^+] (mM)	K_1 (M^{-1})	ΔH_1 (kcal/mol)	N_1	K_2 (M^{-1})	ΔH_2 (kcal/mol)	N_2
*Ec*WT	5	230	$(6.4 \pm 2.0) \times 10^6$	0.1 ± 0.1	1.1 ± 0.1	$(1.2 \pm 0.2) \times 10^5$	-4.4 ± 0.8	0.9
*Ec*WT	10	230	$(4.5 \pm 2.1) \times 10^6$	-0.6 ± 0.1	1.1 ± 0.1	$(3.1 \pm 0.4) \times 10^4$	-5.3 ± 0.2	1.0
*Ec*WT	25	230	$(2.0 \pm 0.9) \times 10^6$	-3.1 ± 0.1	1.0 ± 0.1	$(2.2 \pm 0.3) \times 10^4$	-6.3 ± 0.2	1.0
A1408G	5	150	$(2.3 \pm 0.7) \times 10^6$	1.2 ± 0.1	1.2 ± 0.1	$(1.4 \pm 0.5) \times 10^5$	-0.5 ± 0.1	2.0
A1408G	15	150	$(2.6 \pm 0.3) \times 10^6$	1.6 ± 0.1	1.2 ± 0.1	$(1.6 \pm 0.2) \times 10^5$	-1.4 ± 0.1	2.1
A1408G	25	150	$(1.3 \pm 0.1) \times 10^6$	1.1 ± 0.1	1.2 ± 0.1	$(7.5 \pm 0.7) \times 10^4$	-3.0 ± 0.1	1.8

[a] The values of K, ΔH, and N listed here were derived from the fits of the ITC profiles shown in panels D and H of Figure 2 with a model for two sets of binding sites. The value of N_2 was fixed during each fitting routine and manually varied to yield the best fit (as reflected by minimization of χ^2). The indicated uncertainties reflect the 95% confidence intervals.

The ITC profiles shown in panels D and H of Figure 2 were fit with a model for two sets of binding sites, with the binding parameters derived from these fits being summarized in Table 1. Inspection of these data reveals several significant features. (i) For both *Ec*WT and A1408G, the first binding equilibrium is associated with a binding stoichiometry of approximately one drug molecule per duplex, with the second binding equilibrium being associated with a binding stoichiometry of 1−2 drug molecules per duplex. (ii) When *Ec*WT serves as the host duplex, K_1 (the binding constant associated with the first binding equilibrium) is approximately 53- to 145-fold greater than K_2 (the binding constant associated with the second binding equilibrium), depending on the temperature. Similarly, when A1408G serves as the host duplex, K_1 is approximately 16- to 17-fold greater than K_2. (iii) When *Ec*WT serves as the host RNA, K_1 decreases with increasing temperature. By contrast, when A1408G serves as the host RNA, K_1 is not significantly affected by changes in temperature. (iv) When *Ec*WT serves as the host RNA, the enthalpy associated with the first binding equilibrium (ΔH_1) becomes more negative (exothermic) with increasing temperature, while exhibiting essentially no temperature dependence when A1408G serves as the host RNA.

Paromomycin Binding is Associated with a Negative Change in Heat Capacity When *Ec*WT Serves as the Target Duplex, While Being Associated with Essentially No Change in Heat Capacity When A1408G Serves as the Target Duplex. The heat capacity change (ΔC_p) for a binding interaction can be determined from the temperature dependence of the observed binding enthalpy using the standard relationship:

$$\Delta C_p = \frac{\partial \Delta H}{\partial T} \quad (1)$$

Figure 3 graphically depicts the ΔH_1 data listed in Table 1 in the form of ΔH versus temperature plots. The data points in these plots were fit by linear regression, with the slopes of the resulting lines yielding ΔC_p estimates of -162 ± 5 and -5 ± 26 cal/mol·K for the specific binding of paromomycin to *Ec*WT and A1408G, respectively. Thus, paromomycin binding to *Ec*WT is associated with a negative heat capacity change that falls within a range (−100 to −550 cal/mol·K) that is frequently observed for both ligand−nucleic acid and ligand−protein interactions.[14,15,32−34] In marked contrast, paromomycin binding to A1408G is associated with a heat capacity change of essentially zero. Reductions in solvent-accessible surface area are thought to have an impact on the observed value of ΔC_p,

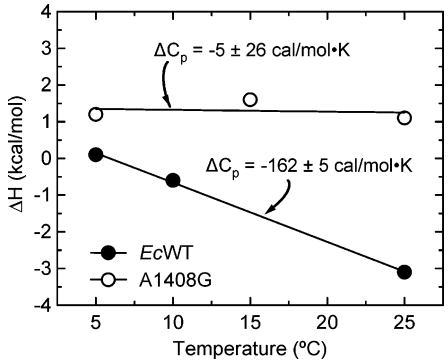

Figure 3. Plots of ΔH versus temperature for the binding of paromomycin to *Ec*WT (●) or A1408G (○). The experimental data points were fit by linear regression analysis, with the resulting fits depicted as solid lines. The values of ΔH used in these plots reflect the ΔH_1 values listed in Table 1.

with the burial of nonpolar surfaces causing ΔC_p values to be more negative and the burial of polar surfaces causing ΔC_p values to be more positive.[2−4,6,10,14,15,34−36] Thus, it is tempting to ascribe the observed difference in ΔC_p for paromomycin binding to *Ec*WT versus A1408G to differential binding-induced alterations in solvent-accessible surface area. In the section that follows, we describe calculations aimed at addressing this possibility.

Calculating Theoretical Heat Capacity Changes for Paromomycin Binding to *Ec*WT and A1408G Based on Binding-Induced Changes in Solvent-Accessible Surface Area. A number of groups have developed formalisms that relate binding-induced changes in both nonpolar and polar solvent-accessible surface areas with ΔC_p. Record and co-workers have characterized the ΔC_p for the folding of various proteins as well as for the transfer of model hydrocarbons and amides from water to the pure liquid phase.[2,3] On the basis of these studies, they have proposed that ΔC_p depends on the accompanying changes in solvent-accessible nonpolar (ΔA_{NP}) and polar (ΔA_P) surface areas (in units of Å^2), according to the following relationship:[2,3]

$$\Delta C_p \text{ (in units of cal/mol·K)} = (0.32 \pm 0.04)\Delta A_{NP} - (0.14 \pm 0.04)\Delta A_P \quad (2)$$

Subsequent studies by Chaires and co-workers on the interactions of duplex DNA with a series of intercalating ligands have resulted in the following revised version of eq 2:[10]

$$\Delta C_p = (0.382 \pm 0.026)\Delta A_{NP} - (0.121 \pm 0.077)\Delta A_P \quad (3)$$

Other studies by the Freire and Murphy groups on the folding of various proteins, as well as the dissolution of different model

(32) Fisher, H. F.; Singh, N. *Methods Enzymol.* **1995**, *259*, 194−221.
(33) Chaires, J. B. *Biopolymers* (*Nucleic Acid Sci.*) **1998**, *44*, 201−215.
(34) Haq, I.; Jenkins, T. C.; Chowdhry, B. Z.; Ren, J.; Chaires, J. B. *Methods Enzymol.* **2000**, *323*, 373−405.

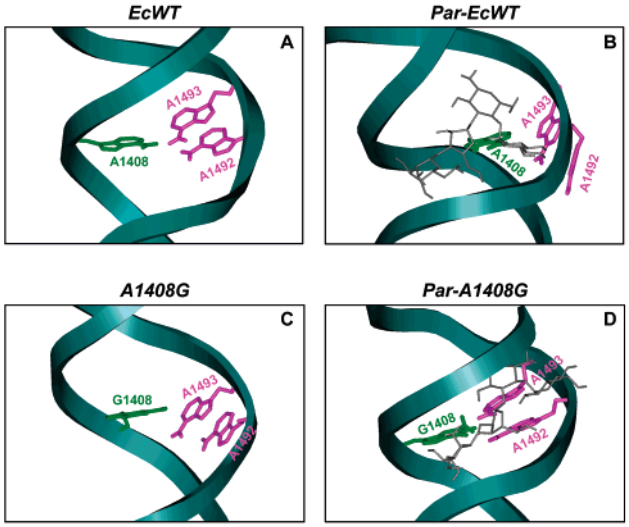

Figure 4. Schematic representations of the solution structures of *Ec*WT and A1408G both in the absence of drug[25,29] (panels A and C, respectively) and in complex with paromomycin[24,29] (panels B and D, respectively). In these renderings, the RNA backbone is depicted in ribbon format. The bases at positions 1492 and 1493 are depicted in magenta, while the base at position 1408 is depicted in green. When present, the drug is depicted in gray.

peptides, have suggested that hydroxyl functionalities behave more like nonpolar surfaces than polar surfaces.[5,6,36] As a result of these studies, a separate term reflecting the change in solvent-accessible hydroxyl surface area (ΔA_{OH}) was introduced, leading to the generation of the following formalism:[4,6,36]

$$\Delta C_p = (0.45 \pm 0.02)\Delta A_{NP} - (0.26 \pm 0.03)\Delta A_P + (0.17 \pm 0.07)\Delta A_{OH} \quad (4)$$

In this equation, as with eqs 2 and 3, the units of ΔC_p are cal/mol·K and the units of all ΔA values are Å^2. Note that in eqs 2 and 3, ΔA_{OH} is included in the ΔA_P term.

Puglisi and co-workers have used NMR techniques to determine the solution structures of *Ec*WT (PDB code 1a3m)[25] and A1408G (PDB code 1fyo),[29] as well as the solution structures of the paromomycin complexes with both host duplexes (PDB code 1pbr for the paromomycin−*Ec*WT complex and 1fyp for the paromomycin−A1408G complex).[24,29] Figure 4 schematically depicts these four structures, which we used to calculate (as detailed in Materials and Methods) the solvent-accessible surface areas [total (A_{TOT}), nonpolar (A_{NP}), polar with hydroxyls (A_{P+OH}), polar without hydroxyls (A_{P-OH}), and hydroxyls (A_{OH})] of the drug-free RNA duplexes, the drug−RNA complexes, and the drug alone (in its RNA bound conformation). The resulting surface areas are listed in Table 2. Table 2 also lists the binding-induced changes in each type of solvent-accessible surface area (ΔA) that we calculated using the following relationship:

$$\Delta A = A_{complex} - (A_{RNA} + A_{drug}) \quad (5)$$

Note that paromomycin binding to both *Ec*WT and A1408G is accompanied by a significant reduction in the total solvent-accessible surface area ($\Delta A_{TOT} = -1094$ Å^2 for the binding to *Ec*WT and −953 Å^2 for the binding to A1408G). Further note that in both cases, the majority of this buried solvent-accessible surface is polar in nature. This latter observation is not surprising since paromomycin, like most aminoglycosides, is highly polar in nature, as are the RNA functionalities that line the major groove where paromomycin binds.

Table 3 lists the theoretical ΔC_p values calculated using the appropriate ΔA data from Table 2 and eqs 2, 3, or 4. Inspection of the ΔC_p data in Table 3 reveals that when either *Ec*WT or A1408G serves as the host duplex, eqs 2−4 yield calculated ΔC_p values of essentially zero, with the actual calculated values (which range from −28 to 46 cal/mol·K) being less than or equal to the uncertainties (which range from 33 to 72 cal/mol·K) inherent in the calculations. Thus, with regard to the impact on ΔC_p, the burial of polar surfaces that accompanies paromomycin binding to each host duplex is effectively offset by the corresponding burial of nonpolar and/or hydroxyl surfaces, thereby yielding a net predicted ΔC_p value of essentially zero.

Calculated Heat Capacity Changes Agree with the Calorimetrically Derived Value Only When A1408G, Not *Ec*WT, Serves as the Host Duplex. Inspection of the data in Table 3 reveals that the calorimetrically derived ΔC_p value of essentially zero (-5 ± 26 cal/mol·K) for paromomycin binding to A1408G is in good agreement with the corresponding calculated ΔC_p values (using eqs 2−4), with the differences between the experimental and calculated values being within the experimental uncertainty. Thus, when A1408G serves as the host duplex, the extent to which paromomycin binding induces the burial of nonpolar and polar solvent-accessible surfaces appears to be a good predictor of ΔC_p. In striking contrast, the calorimetrically derived ΔC_p value of -162 ± 5 cal/mol·K for the binding of paromomycin to *Ec*WT is significantly more negative than the corresponding calculated ΔC_p values of essentially zero. This lack of concordance between experimental and calculated ΔC_p values suggests that the observed negative ΔC_p that accompanies the binding of paromomycin to *Ec*WT is not related to the binding-induced burial of nonpolar solvent-accessible surfaces. Embodied in this notion is the prediction that the binding of paromomycin to *Ec*WT should not be associated with a significant net change in hydration. In the section that follows, we assess the veracity of this prediction using a fluorescence-based osmotic stress approach.

Osmotic Stress Studies Reveal that Paromomycin Binding to *Ec*WT is Accompanied by No Net Change in Hydration. The osmotic stress method has been used extensively to evaluate the participation of water molecules in a wide variety of biochemical reactions.[37,38] One version of this method involves the addition of neutral solutes or cosolvents (osmolytes) to solutions containing the macromolecules and the ligands being studied, thereby altering the water activity of the solution. Typically, one monitors the impact of the osmolyte on the ligand−macromolecule association constant (K_a). An osmolyte-induced increase in K_a reflects a net release of water molecules in conjunction with binding, while an osmolyte-induced decrease in K_a reflects a net uptake of water molecules. We used the osmotic stress method to characterize the hydration changes that accompany the binding of paromomycin to *Ec*WT. An important consideration in the selection of osmolytes is the potential for

(35) Gómez, J.; Freire, E. *J. Mol. Biol.* **1995**, *252*, 337−350.
(36) Luque, I.; Mayorga, O. L.; Freire, E. *Biochemistry* **1996**, *35*, 13681−13688.
(37) Robinson, C. R.; Sligar, S. G. *Methods Enzymol.* **1995**, *259*, 395−427.
(38) Parsegian, V. A.; Rand, R. P.; Rau, D. C. *Methods Enzymol.* **1995**, *259*, 43−94.

Table 2. Solvent-Accessible Surface Areas[a]

molecule	PDB code[b]	A_{TOT} (Å^2)	A_{NP} (Å^2)	A_{P+OH} (Å^2)	A_{P-OH} (Å^2)	A_{OH} (Å^2)
Par−*Ec*WT	1pbr	5312	1375	3937	3246	691
Par alone[c]	1pbr	818	244	574	244	330
Par-free *Ec*WT	1a3m	5588	1364	4224	3520	704
		$\Delta A_{TOT} = -1094$	$\Delta A_{NP} = -233$	$\Delta A_{P+OH} = -861$	$\Delta A_{P-OH} = -518$	$\Delta A_{OH} = -343$
Par−A1408G	1fyp	4944	1202	3742	2997	745
Par alone[c]	1fyp	819	284	535	248	287
Par-free A1408G	1fyo	5078	1189	3889	3265	624
		$\Delta A_{TOT} = -953$	$\Delta A_{NP} = -271$	$\Delta A_{P+OH} = -682$	$\Delta A_{P-OH} = -516$	$\Delta A_{OH} = -166$

[a] Solvent-accessible surface areas were calculated using the GRASP version 1.3 software package[30] with a probe radius of 1.4 Å. A_{P+OH} and A_{P-OH} values reflect the polar solvent-accessible surface areas with and without the inclusion of OH groups, respectively. ΔA values were calculated using eq 5. "Par" denotes paromomycin. [b] PDB[31] codes 1pbr,[24] 1a3m,[25] 1fyp,[29] and 1fyo[29] reflect solution structures derived by NMR. [c] Par alone reflects the structure of paromomycin in its RNA-bound conformation.

Table 3. Calculated (ΔC_p^{Calc}) and ITC-Derived (ΔC_p^{ITC}) Changes in Heat Capacity for the Binding of Paromomycin to the *Ec*WT and A1408G Duplexes

	ΔC_p^{Calc} (cal/mol·K)[a]	ΔC_p^{Calc} (cal/mol·K)[b]	ΔC_p^{Calc} (cal/mol·K)[c]	ΔC_p^{ITC} (cal/mol·K)[d]
*Ec*WT	46 ± 40	15 ± 72	-28 ± 45	-162 ± 5
A1408G	9 ± 38	-21 ± 60	-16 ± 33	-5 ± 26

[a] ΔC_p^{Calc} values were calculated using eq 2, with the indicated uncertainties reflecting the maximal errors in ΔC_p^{Calc} as propagated through the equation. [b] ΔC_p^{Calc} values were calculated using eq 3, with the indicated uncertainties reflecting the maximal errors in ΔC_p^{Calc} as propagated through the equation. [c] ΔC_p^{Calc} values were calculated using eq 4, with the indicated uncertainties reflecting the maximal errors in ΔC_p^{Calc} as propagated through the equation. [d] Calorimetric ΔC_p^{ITC} values were determined from linear regression analyses of the ΔH versus temperature plots shown in Figure 3, with the indicated uncertainties reflecting the standard deviation of the experimental data from the fitted line.

these agents to introduce volume exclusion (i.e., molecular crowding) effects.[39−42] Such effects can alter binding equilibria (typically resulting in an increased association constant) irrespective of any impact from net changes in hydration.[39,42] Thus, one must judiciously select osmolytes so as to alter water activity without introducing volume exclusion effects. We employed ethylene glycol (MW = 62.1 g/mol) and glycerol (MW = 92.1 g/mol) as the osmolytes in our studies since their molecular weights are sufficiently small relative to that of paromomycin so as to minimize the potential for the introduction of volume exclusion effects. Furthermore, these and closely related osmolytes have been used successfully to study water uptake or release in DNA duplex and triplex melting reactions,[43] in the interaction of *gal* repressor with DNA,[44] and in the interactions of intercalating ligands with DNA.[45]

A second important consideration when conducting osmotic stress studies is the impact, if any, of the osmolyte on the structure and stability of the macromolecule target. Control circular dichroism (CD) studies reveal that the structure of *Ec*WT is unaffected by the presence of ethylene glycol and glycerol at the maximum osmolalities used in the osmotic stress studies (Figure S1 in the Supporting Information). Although exerting a negligible impact on the structure of *Ec*WT, the presence of the osmolytes reduces the thermal stability of the host RNA, as revealed by UV melting studies (Figure S2 in the Supporting Information). Spink and Chaires[43] observed similar osmolyte-induced effects on the thermal stabilities of duplex and triplex DNA. In light of the osmolyte-induced reduction in the thermal stability of *Ec*WT, we were careful to conduct our osmotic stress studies at a temperature (5 °C) that ensured an absence of any melted or partially melted duplex molecules.

The target RNA that we used in our osmotic stress studies was a fluorescent form of *Ec*WT in which the adenine at position 1492 (Figure 1B) is substituted with the fluorescent base analogue, 2-aminopurine (2AP). We have previously shown that this substitution alters neither the structure of the RNA duplex nor the affinity of paromomycin for the duplex.[28] We determined paromomycin−RNA K_a values by analyzing the paromomycin-induced change in the fluorescence of the 2AP-labeled RNA (2AP−*Ec*WT) with the following formalism:

$$F = F_0 + \frac{(F_\infty - F_0)}{2}\left[\left([D]_{tot} + [R]_{tot} + \frac{1}{K_a}\right) - \sqrt{\left([D]_{tot} + [R]_{tot} + \frac{1}{K_a}\right)^2 - 4[D]_{tot}[R]_{tot}}\right] \quad (6)$$

In this relationship, F_0 and F are the fluorescence emission intensity of the RNA in the absence and presence of drug, respectively; F_∞ is the fluorescence emission intensity of the RNA in the presence of an infinite drug concentration, and $[D]_{tot}$ and $[R]_{tot}$ are the total concentrations of drug and RNA, respectively. Figure 5 shows representative fluorescence profiles for the titration of paromomycin into a solution of 2AP−*Ec*WT in the absence and presence of ethylene glycol at an osmolality of 6.2. Note that paromomycin binding increases the fluorescence intensity of the host RNA, with the fractional change in intensity per increase in drug concentration being essentially identical in the absence and presence of the osmolyte.

Table 4 lists the K_a values derived from fits of the fluorescence titration profiles shown in Figure 5, as well as K_a values derived from similar fluorescence titration profiles acquired in the presence of ethylene glycol and glycerol at other osmolalities. Inspection of the data in Table 4 reveals a K_a value of $(3.1 \pm 0.4) \times 10^6$ M^{-1} in the absence of osmolyte, a value in good agreement with the corresponding calorimetrically derived value of $(6.4 \pm 2.0) \times 10^6$ M^{-1} listed in Table 1. This agreement between K_a values derived by independent means confirms the negligible impact of the 2AP substitution on paromomycin binding affinity and validates the fluorescence-based technique

(39) Minton, A. P. *J. Biol. Chem.* **2001**, *276*, 10577−10580.
(40) Miyoshi, D.; Nakao, A.; Sugimoto, N. *Biochemistry* **2002**, *41*, 15017−15024.
(41) Sasahara, K.; McPhie, P.; Minton, A. P. *J. Mol. Biol.* **2003**, *326*, 1227−1237.
(42) Hall, D.; Minton, A. P. *Biochim. Biophys. Acta* **2003**, *1649*, 127−139.
(43) Spink, C. H.; Chaires, J. B. *Biochemistry* **1999**, *38*, 496−508.
(44) Garner, M. M.; Rau, D. C. *EMBO J.* **1995**, *14*, 1257−1263.
(45) Qu, X.; Chaires, J. B. *J. Am. Chem. Soc.* **2001**, *123*, 1−7.

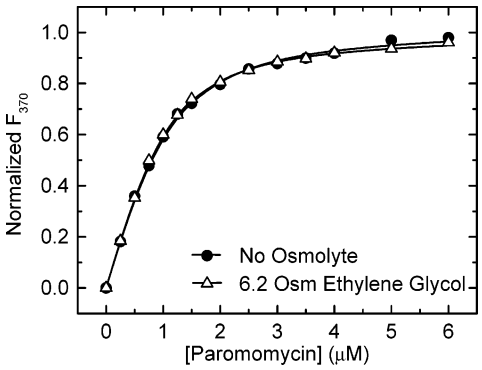

Figure 5. Fluorescence profiles at 5 °C for the titration of paromomycin into a solution of 2AP−*Ec*WT in the absence (●) and presence (△) of ethylene glycol at a concentration of 6.2 Osm. The solid lines represent fits of the experimental data points with eq 6. Solution conditions were 10 mM sodium cacodylate (pH 5.5), 0.1 mM EDTA, and sufficient NaCl to bring the total Na^+ concentration to 230 mM. For clarity of presentation, the fluorescence emission intensity at 370 nm (F_{370}) was normalized by subtraction of the fluorescence intensity in the absence of drug (F_0) and subsequent division by the total calculated binding-induced change in fluorescence ($F_\infty - F_0$).

Table 4. Osmolyte Dependence of the Association Constant at 5 °C for the Binding of Paromomycin to *Ec*WT[a]

osmolyte	osmolality (Osm)	K_a (M^{-1})[b]
none	0	$(3.1 \pm 0.4) \times 10^6$
ethylene glycol	2.1	$(2.8 \pm 0.2) \times 10^6$
ethylene glycol	4.2	$(3.5 \pm 0.3) \times 10^6$
ethylene glycol	6.2	$(3.7 \pm 0.3) \times 10^6$
glycerol	2.2	$(2.5 \pm 0.2) \times 10^6$
glycerol	4.3	$(3.8 \pm 0.5) \times 10^6$
glycerol	6.5	$(3.4 \pm 0.2) \times 10^6$

[a] Solutions conditions were 10 mM sodium cacodylate (pH 5.5), 0.1 mM EDTA, and sufficient NaCl to bring the total Na^+ concentration to 230 mM. [b] Association constants were derived from fits of fluorescence titration profiles, such as those shown in Figure 5, using eq 6. The indicated uncertainties reflect the 95% confidence intervals.

as an alternative approach to ITC for determining aminoglycoside−RNA binding constants.

Further inspection of the data in Table 4 reveals that, at osmolalities up to 6.5, neither the presence of ethylene glycol nor the presence of glycerol exerts any detectable impact on the affinity of paromomycin for the 2AP−*Ec*WT duplex, with the differences between K_a values in the absence and presence of either osmolyte being within the experimental uncertainty. This observation is consistent with the binding of paromomycin to *Ec*WT being accompanied by no net change in hydration. In other words, hydration changes do not appear to provide a significant driving force for the paromomycin−*Ec*WT binding reaction. The generality of this observation with regard to other aminoglycosides remains to be assessed.

The lack of a hydration change accompanying the paromomycin−*Ec*WT interaction supports our calorimetric and computational results described above, which revealed the observed negative ΔC_p for the paromomycin−*Ec*WT interaction to be unrelated to the burial of solvent-accessible surfaces. Westhof and co-workers recently reported a crystal structure (at 2.5 Å resolution) of paromomycin in complex with a model RNA oligonucleotide duplex containing a 16 S rRNA A-site sequence identical to that in *Ec*WT.[27] Significantly, this structure (PDB code 1j7t) reveals 12 hydrogen bonds between the drug and the RNA to be mediated by 8 water molecules. Our osmotic stress results suggest that such water-mediated contacts make use of water molecules that pre-exist in the hydration shells of the free RNA and/or drug, a concept that has been previously suggested by the Westhof group based on an analysis of the hydration patterns in the crystal structures of a multitude of nucleic acids, protein−nucleic acid complexes, and drug−nucleic acid complexes.[46−48]

Binding-Linked Destacking of Adenine Bases Contributes to the Observed Negative ΔC_p that Accompanies the Paromomycin−*Ec*WT Interaction. Our calorimetric, computational, and osmotic stress studies collectively suggest that the observed negative ΔC_p for paromomycin binding to *Ec*WT reflects contributions from one or more factors unrelated to the burial of solvent-accessible surfaces. Furthermore, these contributions are not manifested in the observed ΔC_p for the paromomycin−A1408G interaction. We have previously shown that binding-linked drug protonation reactions contribute significantly to observed negative heat capacity changes for aminoglycoside−rRNA interactions.[12] Lohman and co-workers observed similar effects in studies of single-stranded DNA binding to *E. coli* SSB protein.[9] However, we conducted all of our experimental work at pH 5.5, a pH at which RNA-free paromomycin is essentially fully protonated. These pH conditions should therefore eliminate potential contributions to observed ΔC_p values from coupled drug protonation reactions. Furthermore, such contributions would be manifested in the observed ΔC_p when either *Ec*WT or A1408G serves as the host duplex, an eventuality that is incongruent with our calorimetrically derived ΔC_p data. Thus, it is unlikely that the origin of the negative ΔC_p that we observe for paromomycin binding to *Ec*WT reflects the contributions of binding-linked drug protonation reactions.

The differential values of ΔC_p that we observe for paromomycin binding to *Ec*WT versus A1408G may be related to differences in the impact that paromomycin binding has on the structures of the two host duplexes. A comparison of the NMR-derived solution structures shown in panels A and B of Figure 4 reveals that paromomycin binding to *Ec*WT causes the destacking of the adenine bases at positions 1492 and 1493. Crystallographic studies probing the binding of aminoglycosides (including paromomycin) to 16 S rRNA A-site model oligonucleotides[27,49,50] and an intact 30 S ribosomal subunit[26] have yielded a similar pattern, with the extent of binding-induced base destacking in the crystal structures being even greater than that in the NMR-derived solution structures. Note that A1492 and A1493 are not destacked in the paromomycin−A1408G complex the way they are in the paromomycin−*Ec*WT complex (compare panels B and D of Figure 4). In other words, the adenine base destacking equilibria are coupled to the binding of paromomycin to *Ec*WT, but not to A1408G. We suggest that the origin of our observed negative ΔC_p for the binding of paromomycin to *Ec*WT lies in the destacking of A1492 and A1493 that is coupled to the formation of this complex. In this connection, Kozlov and Lohman[7] have shown that coupled adenine base-destacking equilibria afford significant contributions to the observed negative ΔC_p values for the binding of *E. coli* SSB tetramers to oligoadenylates. These contributions arise from an endothermic adenine destacking enthalpy of ap-

(46) Westhof, E. *Int. J. Biol. Macromol.* **1987**, *9*, 186−192.
(47) Westhof, E.; Dumas, P.; Moras, D. *Biochimie* **1988**, *70*, 145−165.
(48) Auffinger, P.; Westhof, E. *J. Mol. Biol.* **2000**, *300*, 1113−1131.
(49) Vicens, Q.; Westhof, E. *Chem. Biol.* **2002**, *9*, 747−755.
(50) Vicens, Q.; Westhof, E. *J. Mol. Biol.* **2003**, *326*, 1175−1188.

proximately 3.0 kcal/mol per stack,[51] which, in turn, implies a reduction of stacked states at higher temperatures.[52] This temperature-dependent shift in the adenine destacking equilibrium is manifested experimentally as a contribution to the observed negative ΔC_p,[1,7] even if the intrinsic ΔC_p for the base destacking reaction itself is zero, which has been previously suggested.[53] Regarded as a whole, our computational and calorimetric studies suggest that the intrinsic ΔC_p of paromomycin−RNA binding is also near zero. However, the coupling of this binding equilibrium to the adenine base destacking reaction that occurs when *Ec*WT serves as the host duplex results in an *apparent* ΔC_p that is negative. Currently, we are assessing the generality of these observations with regard to other aminoglycosides, which, in turn, will enable us to develop a more complete understanding of the molecular forces that dictate the energetics of aminoglycoside−rRNA recognition.

The coupling of base destacking equilibria to nucleic acid binding is not restricted to aminoglycoside interactions with the 16 S rRNA A-site. For example, drug intercalation into helical (e.g., duplex or triplex) nucleic acid structures is accompanied by the destacking of the repeating base units (e.g., base pairs or base triplets), which is required for insertion of the drug molecules into the helical stack. Chaires and co-workers have used temperature-dependent calorimetric techniques to demonstrate that the binding of a wide variety of intercalating ligands to duplex DNA is associated with a negative ΔC_p.[10] In cases where complementary high-resolution structural information was available, the observed negative ΔC_p values for DNA intercalation correlated well with corresponding values calculated based on the binding-induced burial of solvent-accessible surfaces.[10] However, osmotic stress studies revealed that the DNA intercalation reactions were accompanied by either no net change in hydration or by a net *uptake* of water.[45] These observations are inconsistent with the predicted hydration changes for the burial of solvent-accessible surfaces. Thus, it is unlikely that the observed negative ΔC_p values for the DNA intercalation reactions reflect surface burial alone, if at all. Instead, they may reflect contributions from the base pair destacking equilibria that are coupled to the intercalation reactions.

Concluding Remarks and Implications for Drug Design

The studies described here suggest that the observed negative ΔC_p that accompanies the binding of paromomycin to the prokaryotic 16 S rRNA A-site is the result of contributions from the destacking of A1492 and A1493 that is coupled to complex formation. Furthermore, the binding of paromomycin to rRNA in the absence of such a linked conformational change (as is the case when the eukaryotic 18 S rRNA A-site serves as the target) is associated with an intrinsic ΔC_p of approximately zero. These results have important implications with regard to drug design. Aminoglycoside-induced destacking of A1492 and A1493 in prokaryotic rRNA A-sites is thought to be a determining factor in the deleterious impact the drugs exert on protein synthesis.[26,54] Specifically, the destacked rRNA bases are thought to interact with the minor groove of the minihelix formed the by the tRNA anticodon and the mRNA codon, thereby stabilizing this minihelix (even in the presence of a noncognate anticodon) and causing mistranslation as well as premature termination.[24,26,27,49,54,55] In this regard, the specificity aminoglycosides exhibit for prokaryotic versus eukaryotic rRNA A-sites may reflect the binding-induced destacking of A1492 and A1493 in the prokaryotic sites but not the eukaryotic sites.[28,29] Furthermore, the relative abilities of aminoglycosides or other prokaryotic rRNA A-site targeting compounds to induce the destacking of A1492 and A1493 may correlate with their relative mistranslational and antimicrobial activities. Our results suggest that an observed negative ΔC_p correlates with the binding-induced destacking of A1492 and A1493, thereby providing a calorimetric signature for this biologically important conformational change.

Our heat capacity analysis also has implications with regard to the energetics of drug−macromolecule recognition, in general. The free energy (ΔG_{hyd}) for the hydrophobic transfer of a drug from aqueous solution to its macromolecular binding pocket is a function of the ΔC_p for the binding reaction and is given by the following relationship:[2,3]

$$\Delta G_{hyd} = 80(\Delta C_p) \quad (7)$$

According to this relationship, negative heat capacity changes result in large negative (favorable) ΔG_{hyd} values, which, in turn, provide a significant driving force for complex formation. As an illustrative example, the Chaires and Wilson groups applied eq 7 to show that the major driving force for the binding of various heterocyclic ligands (e.g., Hoechst 33258 and pentamidine) to the minor groove of duplex DNA stems from the hydrophobic transfer of the drugs from solution to the DNA binding site.[14,15,56] Our results indicate that eq 7 should not be applied to binding interactions that are coupled to other temperature-dependent equilibria (e.g., conformational changes or protonation reactions) since such applications result in overestimations of the extents to which hydrophobic effects drive the binding reactions.

Acknowledgment. The calorimetric instrumentation was purchased through funds from NIH Grant S10 RR15959-01. This work was supported by grants from the NIH (CA097123) and the American Cancer Society (RSG-99-153-04-CDD). C.M.B. was supported by an NIH training grant (5T32 GM 08319) in Molecular Biophysics.

Supporting Information Available: CD spectra and UV melting profiles of *Ec*WT in the absence and presence of either 6.2 Osm ethylene glycol or 6.5 Osm glycerol. This material is available free of charge via the Internet at http://pubs.acs.org.

JA0457516

(51) Breslauer, K. J.; Sturtevant, J. M. *Biophys. Chem.* **1977**, *7*, 205−209.
(52) Riley, M.; Maling, B.; Chamberlin, M. J. *J. Mol. Biol.* **1966**, *20*, 359−389.
(53) Filimonov, V. V.; Privalov, P. L. *J. Mol. Biol.* **1978**, *122*, 465−470.
(54) Yoshizawa, S.; Fourmy, D.; Puglisi, J. D. *Science* **1999**, *285*, 1722−1725.
(55) Fourmy, D.; Recht, M. I.; Puglisi, J. D. *J. Mol. Biol.* **1998**, *277*, 347−362.
(56) Wang, L.; Kumar, A.; Boykin, D. W.; Bailly, C.; Wilson, W. D. *J. Mol. Biol.* **2002**, *317*, 361−374.
(57) Recht, M. I.; Fourmy, D.; Blanchard, S. C.; Dahlquist, K. D.; Puglisi, J. D. *J. Mol. Biol.* **1996**, *262*, 421−436.
(58) Recht, M. I.; Douthwaite, S.; Puglisi, J. D. *EMBO J.* **1999**, *18*, 3133−3138.